ELSEVIER

Journal of Volcanology and Geothermal Research 87 (1998) 15–28

Journal of volcanology and geothermal research

# Rheology of bubble-bearing magmas

Michael Manga [a,*], Jonathan Castro [a], Katharine V. Cashman [a], Michael Loewenberg [b]

[a] *Department of Geological Sciences, University of Oregon, Eugene, OR 97403 USA*
[b] *Department of Chemical Engineering, Yale University, New Haven, CT USA*

Received 30 March 1998; accepted 20 July 1998

**Abstract**

The rheology of bubble-bearing suspensions is investigated through a series of three-dimensional boundary integral calculations in which the effects of bubble deformation, volume fraction, and shear rate are considered. The behaviour of bubbles in viscous flows is characterized by the capillary number, *Ca*, the ratio of viscous shear stresses that promote deformation to surface tension stresses that resist bubble deformation. Estimates of *Ca* in natural lava flows are highly variable, reflecting variations in shear rate and melt viscosity. In the low capillary number limit (e.g., in carbonatite flows) bubbles remain spherical and may contribute greater shear stress to the suspension than in high capillary number flows, in which bubble deformation is significant. At higher *Ca*, deformed bubbles become aligned in the direction of flow, and as a result, contribute less shear stress to the suspension. Calculations indicate that the effective shear viscosity of bubbly suspensions, at least for $Ca < 0.5$, is a weakly increasing function of volume fraction and that suspensions of bubbles are shear thinning. Field observations and qualitative arguments, however, suggest that for sufficiently large *Ca* (*Ca* greater than about 1) the effective shear viscosity may be less than that of the suspending liquid. Bubbles reach their quasi-steady deformed shapes after strains of order one; for shorter times, the continuous deformation of the bubbles results in continual changes of rheological properties. In particular, for small strains, the effective shear viscosity of the suspension may be less than that of the liquid phase, even for small *Ca*. Results of this study may help explain previous experimental, theoretical, and field based observations regarding the effects of bubbles on flow rheology. 

*Keywords:* rheology; bubble-bearing magmas; capillary number

## 1. Introduction

Of all the physical properties of magmas that affect their dynamic behaviour, the viscosity of the magma is most variable, varying by over 15 orders of magnitude within the range of natural magma compositions (McBirney, 1993). As a result, numerous studies have considered the effect of various physico-chemical properties on magma rheology, including the effects of composition, temperature, volatile content, crystallinity, and bubble content (e.g., Bottinga and Weill, 1972; Shaw, 1972; Murase and McBirney, 1973; Spera et al., 1988; Bagdassarov et al., 1994). Attempts to determine the effective viscosities in various geologic settings include

* Corresponding author. Tel.: +1-541-346-5574; Fax: +1-541-346-4692; E-mail: manga@newberry.uoregon.edu

0377-0273/98/$19.00 
PII: S0377-0273(98)00091-2

direct measurements (e.g., Pinkerton and Norton, 1995), experimental studies (e.g., Bagdassarov and Dingwell, 1992), and theoretical approaches (e.g., Lange, 1994). Nearly all erupting lavas carry bubbles at some point during their ascent and emplacement. In this paper we use numerical calculations to determine the effect of bubbles on magma rheology.

The present study is motivated by the wide range of experimental results and theoretical models describing the effects of bubbles on the effective viscosity of bubbly magmas. For example, the experimental measurements of Bagdassarov and Dingwell (1992) suggest that the presence of bubbles in rhyolite significantly reduces their effective viscosity. Stein and Spera (1992), however, find that bubbles increase the effective viscosity by an amount that exceeds the increase that would occur for an equivalent volume fraction of solid particles. Theoretical and experimental studies of the effects of bubbles on the rheology of magmas and lavas are reviewed by Stein and Spera (1992).

Inferences drawn from direct observations and field relations of bubble-bearing lavas also provide qualitative and quantitative indications of flow rheology (e.g., Fink, 1984; Lipman and Banks, 1987; Pinkerton et al., 1996). For example, Pinkerton et al. (1996) noted that 'bubble-rich lavas appear more viscous than bubble-poor lavas' in carbonatite flows from Oldoinyo Lengai. Similar observations were made in some Hawaiian lavas (e.g., Hon et al., 1994); however, in some high-velocity basaltic eruptions, bubble-rich lavas appeared to be 'very fluid' relative to bubble-free lavas in the same flow (MacDonald, 1954; Shaw et al., 1968; Lipman and Banks, 1987). While rhyolitic lavas have not been observed to erupt, well-preserved structures in Holocene flows in Oregon and California have been used to infer rheological properties in obsidian and pumiceous lavas (Fink, 1980a, 1984; Castro and Cashman, 1996). Fink (1980a) studied the spacing of pumiceous diapirs in obsidian flows and concluded that the viscosity ratio between pumice and obsidian varied from 50 to 100. While this result is consistent with experimental observations of froth viscosities (e.g., Sibree, 1933), folding relations at Big Glass Mountain as well as at many other flows suggest that obsidian is more viscous than pumice with the same composition (Castro and Cashman, 1996).

In this study we isolate the effects of bubbles on flow rheology through numerical simulations of sus-

Table 1
Melt viscosity and capillary number estimates for viscous deformation of bubbles with a radius of 1 mm

| Lava and flow type | Melt viscosity (PaS) | Capillary number (Ca) |
|---|---|---|
| Carbonatite[a] | $1–10^2$ | 0.02–0.2 |
| Mauna Loa basalt, near vent[b] | $10^2$ | 0.2–1.0 |
| Mauna Loa basalt, distal[b] | $10^2$ | 1.0–5.0 |
| Kilauea basalt[c] | 234–548 | 0.8–1.8 |
| Etna basalt[d] | $10^3$ | 0.1–0.4 |
| Etna basalt[e] | $1.6 \times 10^3$ | 5.4 |
| Mount Spurr, andesite[f] | $10^6$ | 45 |
| Mount St. Helens conduit dacite[g] | $10^7$ | 350 |
| $GeO_2$[h] | $10^4$ | 13–78 |
| Rhyolite[i] | $10^{11}$ | 2–300 |

[a] Viscosity data from Dawson et al. (1994); strain rates from Nakada et al. (1995).
[b] Lipman and Banks (1987).
[c] Pinkerton et al. (1996).
[d] Polacci and Papale (1997).
[e] Kilburn and Guest (1993).
[f] Strain rates were calculated from ascent data presented by Neal et al. (1995).
[g] Rutherford and Hill (1993), and Klug and Cashman (1996).
[h] Stein and Spera (1992).
[i] Bagdassarov and Dingwell (1992) and Pinkerton and Stevenson (1992).

pensions of bubbles. We begin by discussing two parameters that characterize the behaviour of bubbles in viscous flows: the capillary number and the volume fraction of bubbles. Because bubbles will deform in response to viscous stresses, the rheology of bubbly liquids depends on the shear rate $G$. The importance of shear stresses, which act to deform bubbles, relative to surface tension stresses, which tend to keep bubbles spherical, is characterized by the capillary number:

$$Ca = \frac{\mu G a}{\gamma} \quad \text{(capillary number)} \tag{1}$$

where $\gamma$ is the surface tension, $a$ is the undeformed bubble radius and $\mu$ is the suspending fluid viscosity. We also might expect the rheology of bubbly

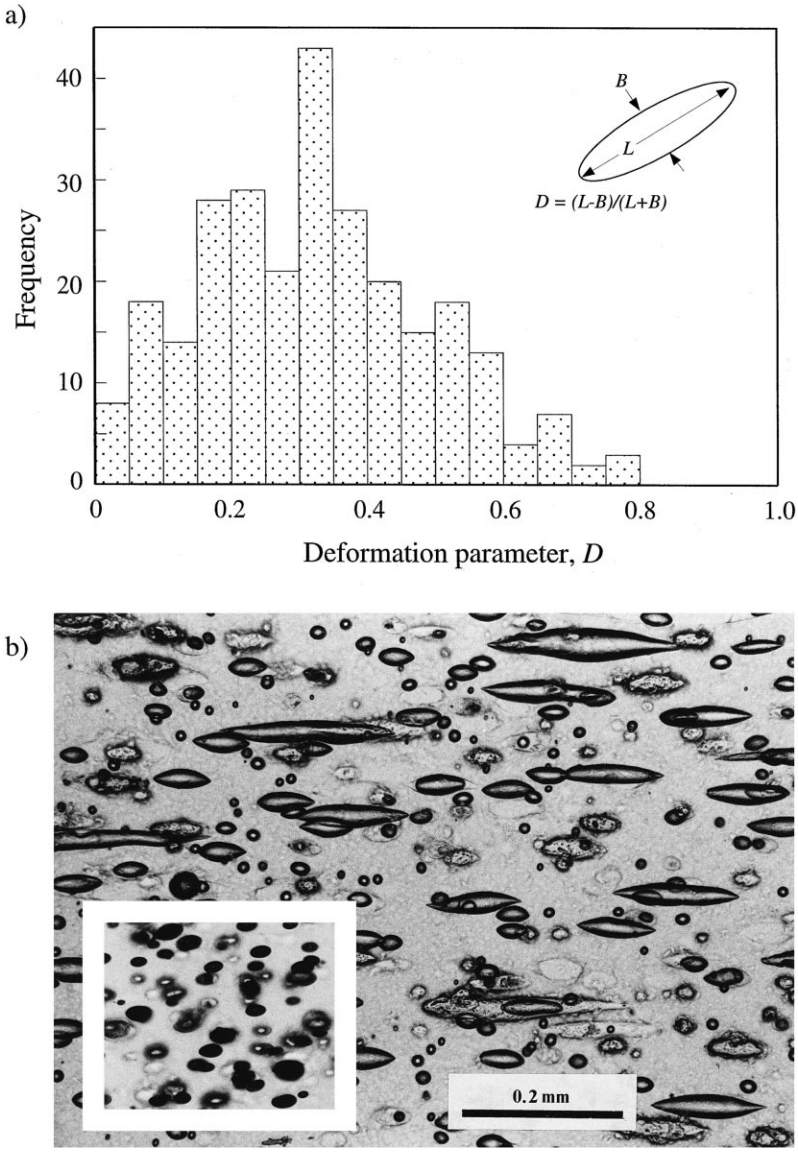


Fig. 1. (a) Distribution of bubble deformation $D$ (see inset for definition) and (b) thin section image from 8 ka obsidian from Mayor Island, New Zealand. The thin was cut parallel to the direction of bubble elongation; the inset shows a thin image of the same sample perpendicular to the larger image.

liquids to depend on the volume fraction of the dispersed bubbles:

$$\phi\,(\text{volume fraction}). \tag{2}$$

In Table 1 we list the range of $Ca$ for various magma compositions and geologic settings assuming a bubble radius of 1 mm. For small $Ca$, the magnitude of bubble deformation, $D=(L-B)/(L+B)$, is approximately equal to $Ca$ (Taylor, 1934); here, $L$ and $B$ are the major and minor axes of the deformed bubble, respectively. For $Ca \gg 1$ the aspect ratio of bubbles scales as $Ca^3$, and the bubbles develop pointed ends (e.g., Stone, 1994). Thus, given the range of $Ca$ in natural magmas and lavas (Table 1) we can expect bubble shapes to range from nearly spherical ($D \approx 0$) in carbonatites and some basalts (e.g., fig. 2 in Cashman et al., 1994) to highly elongated in dacites and rhyolites. In Fig. 1 we present measurements of $D$ for vesicles in a peralkaline rhyolitic clast from the uppermost unit of the 8 ka obsidian flow from Mayor Island, New Zealand. The geology and history of this Mayor Island eruption are described by Stevenson et al. (1993). $D$ was obtained from thin-section images made parallel to the elongation direction, and measurements are based on three-dimensional analysis of bubble shapes. Although vesicle deformation can be large, $D \approx 0.7$, the average deformation is modest, $D \approx 0.3$. The shape of the vesicles preserved in the Mayor Island obsidian may actually be representative of bubble shapes in the molten rock: the pointed ends on the bubbles are preserved even though they will relax most rapidly owing to the high local curvature. The time scale for quenching of the sample must therefore be much shorter than the time scale for relaxation of the deformed bubbles. Also, the inset of Fig. 1b shows that the cross-sections of bubbles are not circular but elliptical, with an aspect ratio consistent with that expected for bubbles in a simple shear flow (e.g., Kennedy et al., 1994).

Here we present the results of numerical simulations of three-dimensional interacting and deforming bubbles in sheared suspensions that allow us to calculate the rheological properties of bubbly liquids as a function of $\phi$ and $Ca$. Due to numerical limitations, we can only compute rheological properties for $0 < \phi < 0.45$ and $0 < Ca < 0.5$. This range of $Ca$, however, is large enough to cover many natural flows, ranging from carbonatites (see Table 1) to rhyolite (see Fig. 1). We are able to explore a sufficiently large range of parameter space to demonstrate that bubble deformation can have a significant effect on the rheological properties of magmas. However, there are also many natural flows in which $Ca$ is larger than the range of values we can study numerically. In §4.2 we thus consider some field observations that provide qualitative results for the limit $Ca \gg 1$.

## 2. Model

Consider a suspension of bubbles, with radius $a$, being sheared at a rate $G$. We assume that flow on the length scale of individual bubbles occurs at low Reynolds number:

$$Re = \rho G a^2/\mu \ll 1, \tag{3}$$

where $\rho$ is the fluid density, and $\mu$ the is the suspending fluid viscosity (Bentley and Leal, 1986). The equations of motion governing flow in the suspending fluid are the Stokes equations:

$$-\nabla p + \mu\nabla^2 \boldsymbol{u} = \boldsymbol{0} \quad \text{and} \quad \nabla \cdot \boldsymbol{u} = 0. \tag{4}$$

Here, $p$ is the pressure and $u$ is the fluid velocity. For simplicity, we assume that buoyancy-driven motion and Brownian motion are negligible compared with flow associated with shearing. We also assume that the bubbles do not change volume.

Across the surface of each bubble, there is a pressure jump $\Delta p$ arising from the surface tension, $\gamma$:

$$\Delta p = \gamma\kappa = \gamma\nabla \cdot \boldsymbol{n}, \tag{5}$$

where $\kappa$ is the local curvature of the bubble surface, and $\boldsymbol{n}$ is a unit normal vector directed outward from the bubble surface. Eq. (5) applies if surface tension is a spatially constant interfacial property. Surface tension may vary over of the surface of the bubble if there are temperature gradients, or if surfactants are present and the concentration of surfactants on the interface is spatially variable. Eq. (4), subject to boundary condition (5), apply at all points in the suspending fluid.

We will consider three classes of models, as illustrated in Fig. 2, each of which allows us to focus

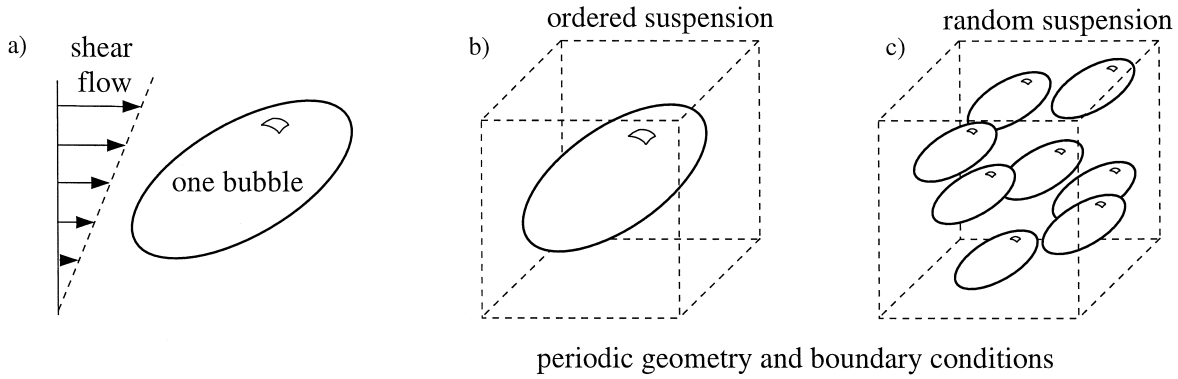


Fig. 2. Geometry of the three problems considered in this study: (a) single bubble, (b) ordered suspension, (c) random suspension. For (b) and (c) we use periodic boundary conditions in all directions.

on different features of the problem. While the model illustrated in Fig. 2c, consisting of a random suspension of bubbles, is the most realistic and relevant model, we are limited in the range of $Ca$ and $\phi$ that can be studied. Calculations for a single bubble (Fig. 2a) allow us to consider larger $Ca$, and calculations for ordered suspensions (Fig. 2b) allow us to study higher $\phi$.

### 2.1. Numerical method

The Stokes equations (Eq. (4)) can be expressed as integral equations, and through the application of the divergence theorem and the Lorenz reciprocal theorem, can be rewritten as sets of equations involving only surface integrals over the surface of all the bubbles (e.g., Rallison and Acrivos, 1978). The resulting integral equations can be solved using standard numerical techniques (e.g., Pozrikidis, 1992). This approach is known as the boundary integral method (BIM), and has the advantage of involving surface integrals and thus requires only a numerical description of the shape of bubbles. Most previous three-dimensional studies of deforming drops and bubbles in suspensions using the BIM approach have been limited to drops with the same viscosity as the surrounding fluid (e.g., Pozrikidis, 1993; Manga, 1997) or single drops (e.g., Rallison, 1984; Kennedy et al., 1994). Here we use the numerical approach of Loewenberg and Hinch (1996) which we found to be more accurate and computationally efficient than the method of Manga and Stone (1995). We verify the accuracy of the Loewenberg and Hinch (1996) code for large bubble deformation by comparing the shapes of bubbles in an axisymmetric extensional flow with those calculated using the numerical procedures described in Manga and Stone (1993). These comparisons are shown in fig. 4 of Loewenberg and Hinch (1996) and fig. 3 of Loewenberg and Hinch (1997).

The BIM is well-suited for problems involving deforming interfaces, in particular, those incorporating interfacial properties such as surface tension. While the BIM allows us to study the motion, deformation, and interaction of the bubbles by focusing only on the surfaces of the bubbles, the method also implicitly solves for the velocity and stresses throughout the bulk of the liquid phase (see Eq. (A9) in Manga and Stone, 1995).

### 2.2. Effect of bubbles on stresses in the suspension

The effective stress tensor for the suspension $\langle \sigma_{ij} \rangle$ is given by the average of the actual stress $\sigma_{ij}$ over a volume $V$ of the suspension:

$$\langle \sigma_{ij} \rangle = \frac{1}{V} \int_V \sigma_{ij} \mathrm{d}V. \tag{6}$$

Following Batchelor (1970) and Pozrikidis (1993), if the suspending fluid is Newtonian and the flow occurs at low Reynolds numbers, then:

$$\langle \sigma_{ij} \rangle = -\delta_{ij} < p > + 2\mu < e_{ij} > + \frac{1}{V} \int_{S_b} \left[ 2\gamma\kappa n_i x_j - \mu(u_i n_j + u_j n_i) \right] \mathrm{d}S, \tag{7}$$

where $S_b$ indicates the surfaces of all the bubbles in the suspension, $e_{ij}$ is the rate-of-strain tensor, $\boldsymbol{x}$ is a position vector, $\boldsymbol{n}$ is again a unit normal vector directed outward from the bubbles, and $\langle\ \rangle$ indicates a volume-averaged quantity. The velocity $\boldsymbol{u}$, and the shape of the bubbles used to calculate $\kappa$, are determined by solving the integral equation representation of Stokes equations (see Section 2.1). The last term on the right-hand side (RHS) of Eq. (7) represents the additional stresses contributed by the suspended bubbles.

We normalize stresses by the viscous shear stress $\mu G$, lengths by $a$, velocities by $Ga$, and time by $1/G$. The additional normalized stresses due to the dispersed bubbles, hereafter denoted by the tensor $\Sigma_{ij}$, are given by:

$$\Sigma_{ij} = \frac{3\phi}{4\pi}\int_{S_b}\left[\tfrac{2}{Ca}\kappa n_i x_j - (u_i n_j + u_j n_i)\right] dS, \qquad (8)$$

where all quantities on the RHS are now dimensionless.

The shear viscosity of the suspension, relative to that of the suspending liquid, is given by:

$$\mu_{rel} = 1 + \Sigma_{12} = \frac{\text{effective viscosity of bubbly fluid}}{\text{viscosity of suspending fluid}}. \qquad (9)$$

Normal stress differences will also result from bubble deformation. These non-dimensional quantities are defined as (e.g., p. 56 in Leal, 1992):

$$N_1 = \Sigma_{11} - \Sigma_{22} \text{ and } N_1 = \Sigma_{22} - \Sigma_{33}. \qquad (10)$$

Eq. (7) is in fact valid only if the suspended bubbles are force-free, so that the last integral on the RHS is independent of the choice of the origin. For the problem considered here, stresses associated with the shear flow are assumed to be much greater than those due to density differences.

### 2.3. Solution details

In order to solve the integral equations, we describe the shape of each bubble with a deforming mesh of triangles (Loewenberg and Hinch, 1996). We use 1620 triangles for single bubble calculations (Fig. 2a), 1280 triangles for the ordered suspension (Fig. 2b), and 500 triangles on each bubble for the random suspension (Fig. 2c). As the number of triangles increases, the accuracy of the calculations increases; Loewenberg and Hinch (1996, 1997) provide a detailed discussion of the numerical error resulting from discretizing the surface of the bubbles. In the random suspension we use 8 bubbles. Calculations with 6 and 12 bubbles produce essentially identical results.

To describe the time-evolution of bubble shape and position, we time-integrate the velocity at interfacial grid points (nodes of triangles) on the surface of each bubble. For the single bubble problem, we run the calculations until a steady shape is reached. For the ordered and random suspensions, rheological properties vary periodically in time, as shown by Pozrikidis (1993); thus we run the calculations for a sufficiently long time that we can time-average quantities. Small temporal fluctuations of rheological properties (see Fig. 9 shown later) are due to temporal changes in the relative positions of the bubbles and their resulting interactions. Typical computation times on an UltraSparc 2 for a single simulation of each of the three problems shown in Fig. 2 are about 2, 5 and 10 h, respectively.

## 3. Results

In Fig. 3a we show the added shear stress $\Sigma_{12}/\phi$ due to a single bubble, corresponding to $\phi \ll 1$, as a function of the capillary number. $\Sigma_{12}$ is divided by $\phi$ in order to facilitate comparisons between results; $\Sigma_{12}/\phi$ is proportional to the added shear stress per bubble. As $Ca$ increases (corresponding to an increasing shear rate), $\Sigma_{12}$ decreases, implying that fluids containing deformable bubbles are shear thinning. As $Ca$ increases, the magnitude of deformation increases as shown in Fig. 2b. Taylor (1934) determined the deformation of a single bubble in a shear flow, with the measure of distortion defined as $D = (L - B)/(L + B)$ (see inset of Fig. 3b for definitions of $L$ and $B$) so that $0 \le D < 1$. For small values of $Ca$, $D = Ca$ (Taylor, 1934), in agreement with the numerical results for the full range $0 < Ca \le 0.5$ considered here. For $Ca \gg 1$, bubbles become highly elongated with an aspect ratio $L/B \sim Ca^3$ (e.g., Stone, 1994). Our numerical procedure, at least for three-dimensional bubbles, does not allow us to cal-

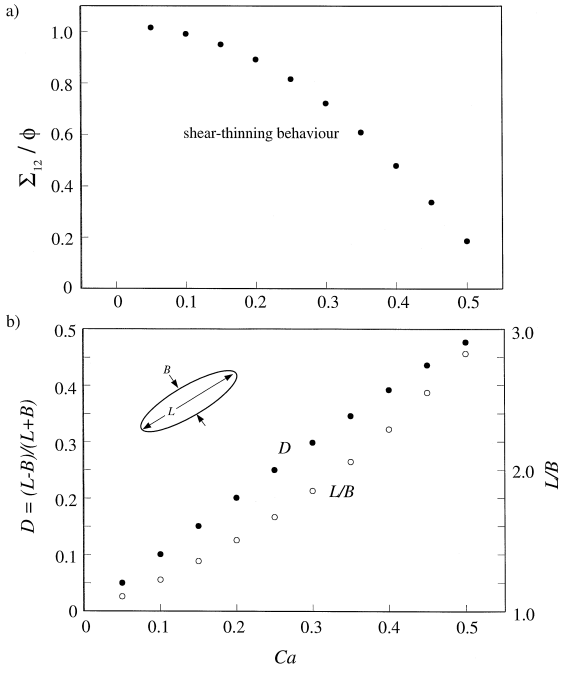


Fig. 3. (a) Shear stress, $\Sigma_{12}/\phi$, and (b) bubble deformation $D$ (see inset) as a function of $Ca$ for a single bubble (Fig. 2a).

culate the high curvature associated with the pointed ends of highly deformed bubbles and thus limits our calculations to $Ca \leq 0.5$.

In Fig. 4 we show the added shear stress $\Sigma_{12}/\phi$ as a function of $\phi$ for $Ca = 0.3$ in an ordered suspension. For comparison we show $\Sigma_{12}/\phi$ for a suspension of rigid spheres assuming that the relative

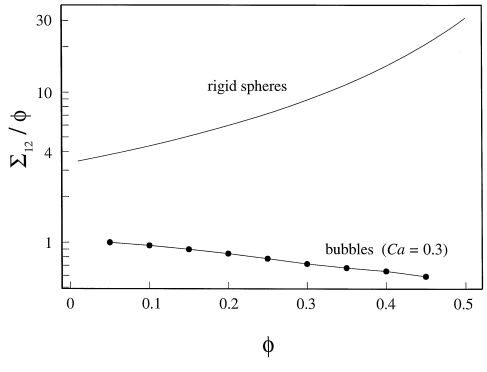


Fig. 4. Shear stress, $\Sigma_{12}/\phi$, as a function of $\phi$ in an ordered suspension (Fig. 2b) for $Ca = 0.3$. For comparison, the shear stress in a suspension of rigid spheres is shown.

viscosity, $\mu_{rel}$, of the suspension of spheres is given by (e.g., Roscoe, 1952):

$$\mu_{rel} = (1 - 1.35\phi)^{-5/2}. \quad (11)$$

Eq. (11) is similar to typical expressions for the $\phi$-dependence of $\mu_{rel}$ for non-Brownian spheres (see Russel et al., 1989 Chap. 14). As $\phi$ increases and bubble–bubble interactions become more important, the contribution of each bubble to the shear stress decreases. By contrast, particle–particle interactions between solid spheres increase the shear stress associated with each sphere.

In Fig. 5a we consider the effects of both $\phi$ and $Ca$ on the shear stress $\Sigma_{12}/\phi$ for the case of a random suspension. The results are consistent with those shown in Fig. 3 in that suspensions of bubbles are shear thinning. Also, the shear stress contributed

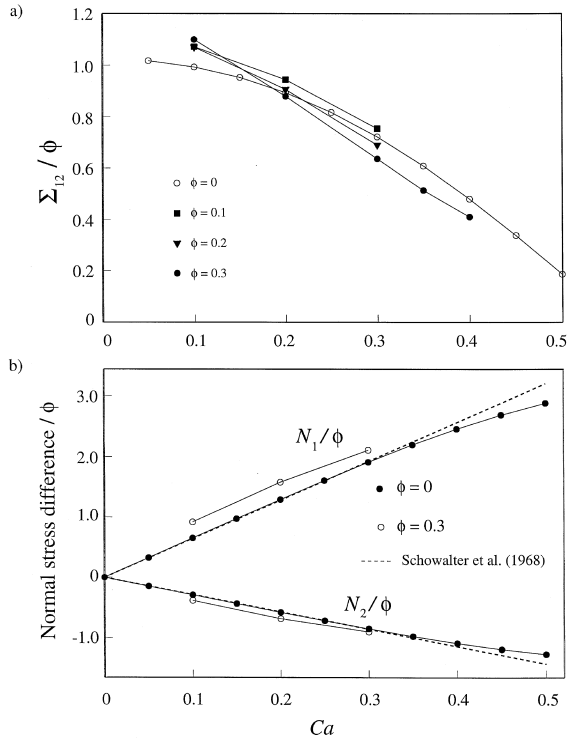


Fig. 5. (a) Shear stress, $\Sigma_{12}/\phi$, as a function of $Ca$ for a random suspension with eight bubbles, and $\phi = 0.1$, 0.2 and 0.3. Points for $\phi = 0$ are for the single bubble calculation (Fig. 1a). (b) Normal stress differences, Eq. (10), as a function of $Ca$ for a random suspension with eight bubbles and $\phi = 0.3$. Points for $\phi = 0$ are for the single bubble calculation.

by each bubble decreases as the volume fraction increases, at least for $Ca$ greater than about 0.1.

Finally, in Fig. 5b we show computed normal stress differences, $N_1/\phi$ and $N_2/\phi$, along with the normalized analytical solutions of Schowalter et al. (1968) valid for small $Ca$:

$$N_1/\phi = \frac{32}{5} Ca \quad \text{and} \quad N_2/\phi = -\frac{20}{7} Ca. \qquad (12)$$

In Eq. (12), as before, stresses are normalized by $\mu G$. The numerical results deviate (slightly) from the Schowalter et al. (1968) results for $Ca$ greater than about 0.4. In a Newtonian fluid without bubbles these normal stress differences would be zero. They are non-zero here due to the deformation of the bubbles. In fact, their magnitude can become a substantial fraction of the shear stress which suggests that caution should be used in modeling magmas containing deformable bubbles as Newtonian fluids, as noted previously by Spera et al. (1988). For example, if $\phi = 0.3$ and $Ca = 0.3$, the first normal stress difference is about half the total shear stress.

## 4. Discussion

The numerical results in Figs. 3 and 5 are consistent with experimental measurements of the shear thinning behaviour of bubbly liquids (e.g., Shaw et al., 1968). A physical explanation for this behaviour is illustrated in Fig. 6a. The extra shear stress contributed by bubbles is due to the additional viscous dissipation occurring within the fluid that must flow over and around the bubbles. For spherical bubbles, the distortion of streamlines and the associated viscous dissipation is greater than that for deformed and elongated bubbles.

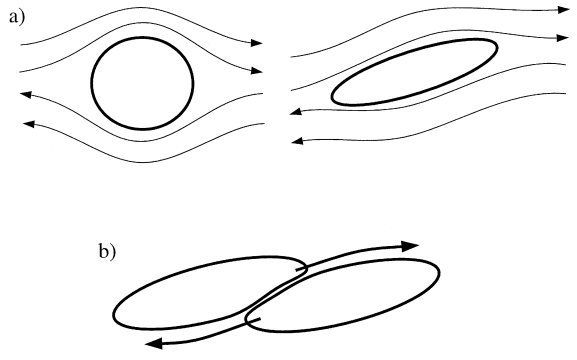


Fig. 6. (a) Illustration of bubble shapes and streamlines for small $Ca$ (left) and high $Ca$ (right). Deformed bubbles result in less deformed streamlines, and thus less viscous dissipation. (b) Deformed bubbles can 'slide' over each other more easily than spherical bubbles.

In Figs. 4 and 5 we noted that for $Ca > 0.1$, the contribution of each bubble to the total shear stress decreases as $\phi$ increases. A physical explanation is illustrated in Fig. 6b. As $\phi$ increases, bubbles are forced to slide over and around each other. Because the surface of the bubble is a free-slip boundary, that is, the surface offers no shear resistance (as opposed to the no-slip surface on rigid particles), deformable bubbles can slide over each other. As a result, the dissipation of energy in the region between the bubbles is reduced.

### 4.1. Effective viscosity of bubbly magmas

In Fig. 7 we compare the relative shear viscosity, $\mu_{rel} = 1 + \Sigma_{12}$, based on our calculations with values obtained from other models and experimental measurements. We show numerical results for $Ca = 0.3$ for both ordered and random suspensions (filled and open symbols, respectively). The curve labeled 'Stein and Spera' is the best-fit line for experimental measurements in $GeO_2$ for $Ca \gg 1$ and $\phi < 0.055$ (Stein and Spera, 1992). Three theoretical models are shown: Taylor (1932) valid for $\phi \ll 1$ and spherical bubbles; Dobran (1992); Jaupart and Allègre (1991). We find that bubbles, even for the modest deformations that arise for $Ca = 0.3$, have a small effect on the suspension's viscosity, with $\mu_{rel}$ increasing by only about 25% for a volume fraction of 0.45.

The model used by Jaupart and Allègre (1991) is consistent with the experimental measurements of Sibree (1933) for bubbly liquids. However, the 'froths' studied by Sibree were stabilized by an organic colloid that produces absorption layers on the surface of the bubbles. It is possible that the reduced mobility of these layers made the bubbles behave more like rigid particles. Indeed, the measurements of Sibree, and the model of Jaupart and Allègre, are similar to typical models for suspensions of rigid spheres.

The experimental measurements of Stein and Spera (1992) are more puzzling because at high

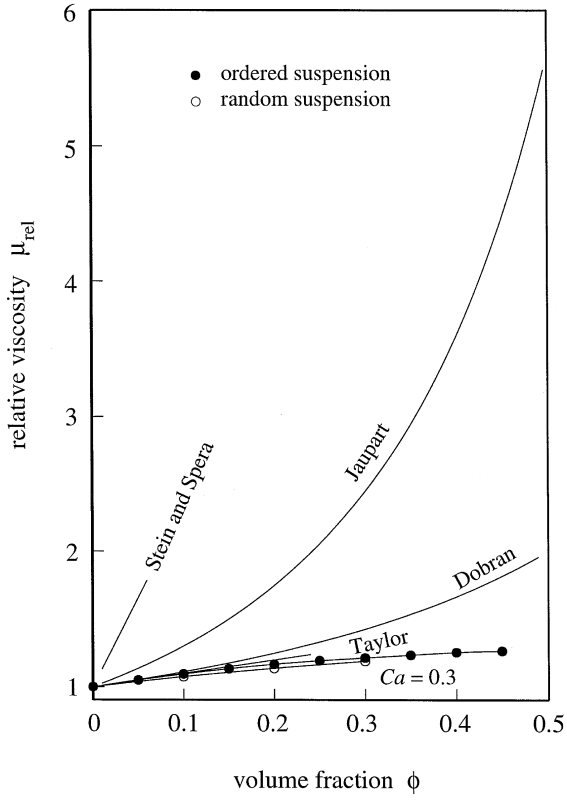


Fig. 7. Relative viscosity, Eq. (9), as a function of volume fraction $\phi$ for various models. Results of this study for Ca = 0.3 are shown for ordered (solid disks) and random (open circles) suspensions. Other results are shown with solid curves: Taylor (1932), valid for spherical bubbles and low volume fractions; Dobran (1992); Jaupart and Allègre (1991); experimental results of Stein and Spera (1992).

capillary numbers the effect of bubbles is reduced (see Figs. 3a and 5a). Yet, the Stein and Spera measurements suggest a viscosity increase that is even greater than that for a suspension with the same volume fraction of solid spheres. One possible explanation is that the highly deformed bubbles in the Stein and Spera samples contributed to the shear stress by behaving as long thin rigid particles, perhaps due to quenching or crystallization on the surface of the bubbles. The relative viscosity of a suspension of rods with $\phi = 0.05$ and aspect ratio 20 in a simple shear flow is $\approx 1.4$ (Shaqfeh and Fredrickson, 1990), similar to $\mu_{rel} = 1.66$ predicted by the Stein and Spera best fit curve for $\phi = 0.05$.

In summary, the theoretical results presented in Section 3 indicate that the relative viscosity of a suspension of bubbles is a weakly increasing function of volume fraction. In addition, suspensions of bubbles are shear thinning.

### 4.2. High shear rates ($Ca \gg 1$)

The estimates of *Ca* for natural flows (Table 1) indicate that in some cases *Ca* is greater than (and sometimes even much greater than) one. Unfortunately, the pointed ends that develop on bubbles for *Ca* greater than about 0.5 prevent us from calculating rheological properties at these conditions. However, in the limit that $Ca \gg 1$, we can develop some scaling estimates for $\mu_{rel}$. Consider a suspension of bubbles in a simple shear flow. Assuming that surface tension is negligible ($Ca \gg 1$) and that streamlines are not distorted by the bubbles, viscous dissipation occurs only in the liquid phase so that $\mu_{rel} = 1\text{-}\phi$. Thus, in contrast to the $Ca < 0.5$ limit we considered numerically in which $\mu_{rel} > 1$, if *Ca* is sufficiently large then $\mu_{rel}$ may be $< 1$.

Here we consider a set of observations of small scale folds in rhyolitic obsidian lavas that indicate that the relative shear viscosity may indeed be less than one for $Ca \gg 1$. If the liquid viscosity is $10^{11}$ Pa s (Webb and Dingwell, 1990), the surface tension $\gamma \approx 0.2$ N/m (Murase and McBirney, 1973), and a typical bubble radius is 1 mm, then *G* would have to be less than about $2 \times 10^{-9}$ $s^{-1}$ for *Ca* to be less than 1. This shear rate is two orders of magnitude smaller than the lower bound of estimated shear rates associated with large scale surface folds in obsidian flows (Fink, 1980b). In fact, at such low strain rates, it would take about 50 years to produce the folds we consider in this section (an unreasonably long time) suggesting that *Ca* is indeed $\gg 1$.

Centimeter-scale fold structures in late Holocene flows (e.g., Big Glass Mountain, CA, and Big Obsidian Flow, OR) provide evidence of the relative viscosities of bubbly rhyolitic lavas. Fig. 8 depicts a ptygmatically folded obsidian layer within a matrix of coarsely vesicular pumice from Big Glass Mountain, CA. Ptygmatic fold structures are typically produced by buckling of a highly viscous layer in a less viscous matrix (Ramsay and Huber, 1987). As the assemblage depicted in Fig. 8 was shortened, the

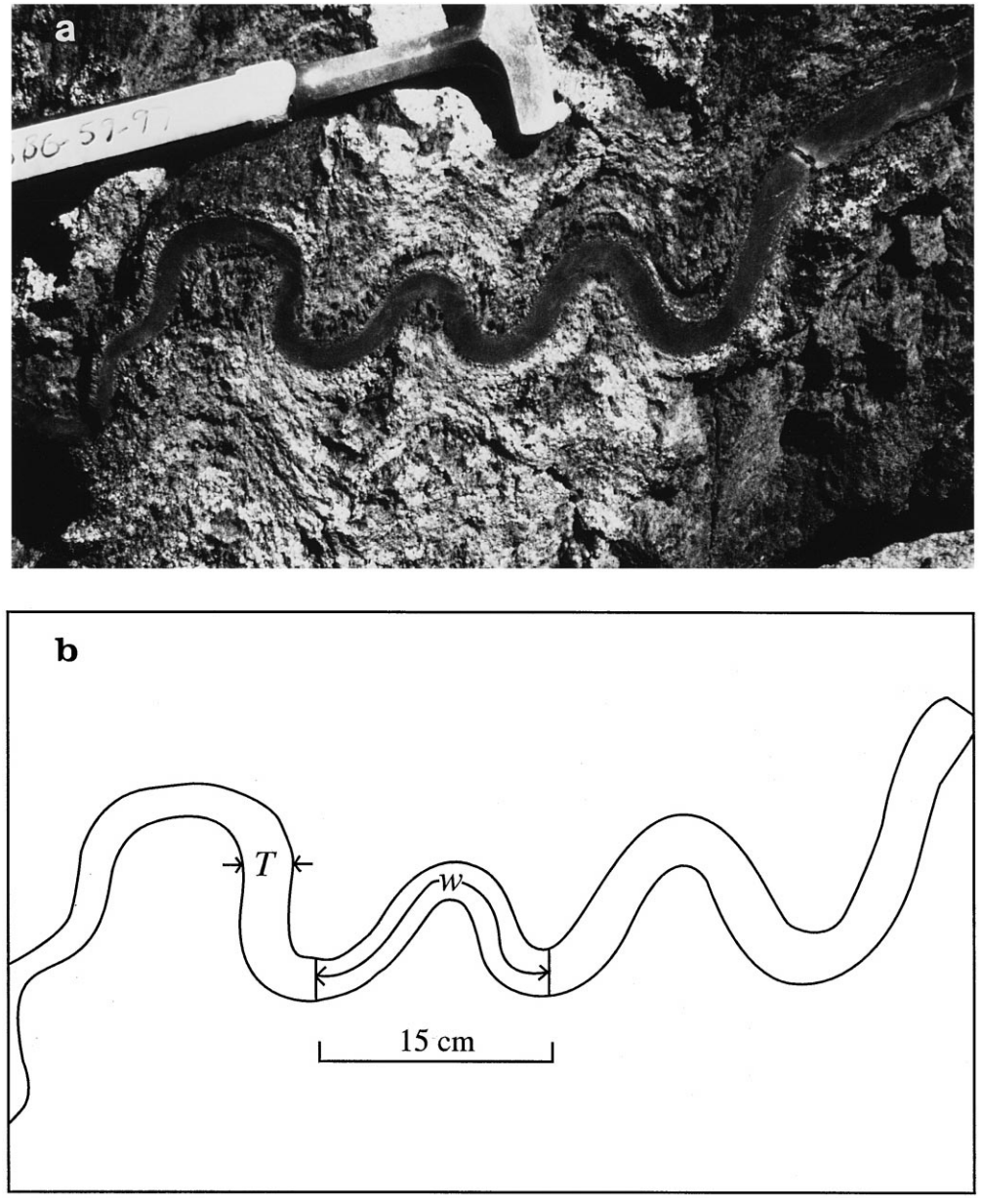


Fig. 8. (a) Glassy obsidian layer, $\phi \approx 0$, folded in coarsely vesicular pumice, $\phi \approx 0.5$, from Big Glass Mountain, CA. (b) Trace of the fold structure showing thickness, $T$, and arc wavelength, $w$, of the folded layer. $\mu_1$ and $\mu_2$ are the viscosities of the folded obsidian layer and the pumiceous matrix, respectively. Measurements of wavelength and thickness from this sample indicate that the relative viscosity of the bubbly matrix is $\mu_{rel} = \mu_2/\mu_1 \approx 0.3$.

obsidian layer ($\phi \approx 0$) buckled while the bubble-rich ($\phi \approx 0.5$) matrix deformed around the fold. Thus, the geometry of these structures is a consequence of the obsidian layer having a higher viscosity than the pumiceous medium, i.e., $\mu_{rel} < 1$. Indeed, all buckle folds observed in obsidian flows are less vesicular than their surrounding matrices (Castro and Cashman, 1996). Here we estimate the relative viscosity

of the vesicular and glassy lavas by applying buckling theory (Biot, 1961) to folded obsidian-pumice assemblages.

According to buckling theory, the dominant arc wavelength $w$ of a single layer fold is established at the onset of deformation and is a function of the layer thickness $T$ and the relative viscosity of the bubble-rich lava, $\mu_{rel}$ (Biot, 1961). Assuming the folded layer is bubble-free, the relationship between $\mu_{rel}$ and the fold wavelength is expressed by (e.g., Biot, 1961):

$$\mu_{rel} = 42\left(\frac{T}{w}\right)^3. \quad (13)$$

The relationship between $\mu_{rel}$ and fold geometry described by Eq. (13) assumes that both the folded material and surrounding matrix are Newtonian fluids and that the bubbles do not change volume during deformation. In addition, folding was probably produced by a flow more closely resembling pure shear than the simple shear considered in this paper. Provided $Ca$ is very large and strains are small (limits that apply for the folds considered here), the surface tension stresses that produce the normal stresses in Fig. 5b will be small, and the Newtonian model may actually be a reasonable approximation. Given the limitations of Newtonian buckling theory, we will use the Biot (1961) model merely as a preliminary attempt to interpret the observed geometries of glassy folds from Big Glass Mountain, CA.

Measurements of the relationship between $w$ and $T$ for the fold in Fig. 8 suggest that $\mu_{rel} \approx 0.3$. Other values of $\mu_{rel}$ for single layer glassy folds from Big Glass Mountain are listed in Table 2. We consider only samples in which folded layers are separated by many fold wavelengths so that no other folds influence the folding. For all folds examined, $0.002 < \mu_{rel} < 0.3$. While we would be overly optimistic to assume that $\mu_{rel}$ obtained by the application of the Biot (1961) folding analysis is quantitatively informative, at least qualitatively, bubbly rhyolite appears to be much less viscous than bubble-free rhyolite. Such viscosity contrasts are most likely a consequence of the presence of bubbles given that the composition and crystallinity are indistinguishable between the obsidian and pumice (Laidley and McKay, 1971; Fink, 1982; Grove and Donelly-Nolan, 1986).

In contrast to the results of numerical calculations presented in Section 3, folding analysis of structures in obsidian flows suggest that the relative viscosity of bubbly rhyolite may be less than one. Experimental measurements of Bagdassarov and Dingwell (1992) for $Ca > 1$ also indicate that $\mu_{rel} < 1$, and that with increasing volume fraction the relative viscosity decreases as $\mu_{rel} = (1 + 22.4\phi)^{-1}$. The magnitude of the decrease, however, is much greater

Table 2
Measured and computed parameters on obsidian folds from Big Glass Mountain, CA

| Sample | Thickness[a] $T$ (cm) | Wavelength $w$ (cm) | Shortening (%) | $\phi$[b] | $\mu_{rel}$ |
|---|---|---|---|---|---|
| SBG-1 | 0.46 | 4.8 | 42 | 47 | 0.04 |
| SBG-3 | 1.1 | 22.1[c] | 55 | ≈ 50[d] | 0.005 |
| SBG-55 | 0.78 | 7.6 | 51 | 67 | 0.05 |
| SBG-41a | 0.44 | 5.1 | 41 | 74 | 0.03 |
| SBG-41b | 0.11 | 2.9 | 47 | 74 | 0.002 |
| SBG-69 | 1.3 | 16.3 | 54 | N.A.[e] | 0.02 |
| SBG-59 | 0.37 | 4.0 | 37 | N.A.[e] | 0.03 |

[a] Based on an average of about 10 measurements.
[b] Porosities were calculated from density measurements using the techniques of Houghton et al. (1988) and are determined from the average of 30 density measurements.
[c] Average of four wavelengths whose standard deviations is 3.1 cm.
[d] Based on close proximity to SBG-1.
[e] Folding analysis based on photographs only.

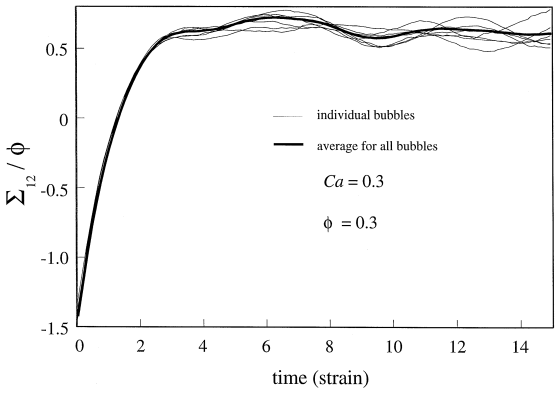


Fig. 9. Temporal change in the shear stress, $\Sigma_{12}/\phi$, in a random suspension (Fig. 2c) with 8 bubbles, $Ca = 0.3$ and $\phi = 0.3$. Time is normalized by the shear rate so that a time of 1 corresponds to a strain of 1. The thin curves are values for individual bubbles and the bold curve is the average value.

than our $1 - \phi$ estimate made at the beginning of this section.

### *4.3. Transient effects*

The rheological measurements presented in Figs. 3–5 and 7 are quasi-steady results which are obtained after total strains of about 1–4, as shown in Fig. 9 (time is normalized by the shear rate so that a dimensionless time of 1 implies a strain of 1). As *Ca* increases, the strain required for $\mu_{rel}$ to reach a steady value increases. In Fig. 9, the bold curve is the average value of $\Sigma_{12}$ and the thin curves are values of $\Sigma_{12}$ for each of the eight bubbles. The oscillations of $\Sigma_{12}$ are due to temporal variations of the relative positions of the bubbles in the sheared suspension.

Our calculations thus indicate that strains of greater than order 1 are necessary to obtain steady rheological measurements due to the transient evolution of bubble microstructure. For comparison, the Bagdassarov and Dingwell (1992) measurements are for strains of about 0.02; the relative shear viscosities inferred from the folding analysis presented in this paper are based on folded structures that represent strains of about $1/2$. In both cases, it is thus likely that the inferred viscosities are in fact transient properties.

## 5. Concluding remarks

The rheology of bubble-bearing magmas is a function of the volume fraction of bubbles and the amount of deformation. Results of three-dimensional boundary integral calculations indicate that the effective viscosity of bubble-bearing magmas is only a slightly increasing function of volume fraction, in contrast to the behaviour of suspensions of rigid particles. As the volume fraction increases, the distance between bubbles decreases and bubbles can slip over each other. Calculations also indicate that with increasing capillary number and deformation bubbles become aligned in the flow direction and contribute less shear stress to the suspension when compared to spherical bubbles. For strains of less than order one, the effective shear viscosity and other rheological properties vary with time due to changes in the shape of the bubbles. Steady rheological properties occur only once the bubbles have deformed to near-steady shapes.

## Acknowledgements

M.M. is supported by a NSF CAREER grant. M.L. acknowledges support from NSF grant CTS-9624615 and NASA grant NAG 3-1935. K.V.C. acknowledges support from NSF award EAR9614753. Additional support was provided by the Donors of the Petroleum Research Fund, administered by the American Chemical Society, through a grant to M.M. Reviews and comments by F. Spera and an anonymous reviewer improved this manuscript.

## References

Bagdassarov, N., Dingwell, D.B., 1992. A rheological investigation of vesicular rhyolite. J. Volcanol. Geotherm. Res. 50, 307–322.

Bagdassarov, N.S., Dingwell, D.B., Webb, S.L., 1994. Viscoelasticity of crystal- and bubble-bearing melts. Phys. Earth. Planet. Inter. 83, 83–99.

Batchelor, G.K., 1970. The stress system in a suspension of force-free particles. J. Fluid Mech. 41, 545–570.

Bentley, B.J., Leal, L.G., 1986. An experimental investigation of

drop deformation and breakup in steady two-dimensional linear flows. J. Fluid Mech. 167, 241–283.
Biot, M.A., 1961. Theory of folding of stratified viscoelastic media and its implication in tectonics and orogenesis. Geol. Soc. Am. Bull. 72, 1595–1620.
Bottinga, Y., Weill, D.F., 1972. The viscosity of magmatic silicate liquids. Am. J. Sci. 272, 438–475.
Cashman, K.V., Mangan, M.T., Newman, S., 1994. Surface degassing and modifications to vesicle size distributions in active basalt flows. J. Volcanol. Geotherm. Res. 61, 45–68.
Castro, J.M., Cashman, K.V., 1996. Rheologic behavior of obsidian and coarsely vesicular pumice in Little Glass Mountain and Obsidian Dome California. EOS 77, 802.
Dawson, J.B., Pinkerton, H., Pyle, D.M., Nyamweru, C., 1994. June 1993 eruption of Oldoinyo Lengai, Tanzania: exceptionally viscous and large carbonatite lava flows and evidence for coexisting silicate and carbonate magmas. Geology 22, 799–802.
Dobran, F., 1992. Nonequilibrium flow in volcanic conduits and application to eruptions of Mt St Helens on May 18, 1980, and Vesuvius in AD 79. J. Volcanol. Geotherm. Res. 49, 285–311.
Fink, J.H., 1980a. Gravity instability in the Holocene Big and Little Glass Mountain rhyolitic obsidian flows Northern California. Tectonophysics 66, 147–166.
Fink, J.H., 1980b. Surface folding and viscosity of rhyolite flows. Geology 8, 250–254.
Fink, J.H., 1982. Surface structure of Little Glass Mountain. In Guides to Some Volcanic Terranes in Washington, Idaho, Oregon, and Northern California. U.S. Geol. Surv. Circ. 939, 171–176.
Fink, J.H., 1984. Structural geologic constraints on the rheology of rhyolitic obsidian. J. Non-Crystal. Solids 67, 135–146.
Grove, T.L., Donelly-Nolan, J.M., 1986. The evolution of young silicic lavas at Medicine Lake Volcano, California: Implications for the origin of compositional gaps in calc-alkaline series lavas. Contrib. Mineral. Petrol. 92, 281–302.
Hon, K., Kauahikaua, J., Denlinger, R., Mackay, K., 1994. Emplacement and inflation of pahoehoe sheet flows: Observations and measurements of active lava flows on Kilauea Volcano Hawaii. Geol. Soc. Am. Bull. 106, 351–370.
Houghton, B.F., Wilson, C.J.N., Hassan, M., 1988. Density measurements for pyroclasts and pyroclastic rocks. New Zealand Geol. Surv. Rec. 35, 73–76.
Jaupart, C., Allègre, C.J., 1991. Gas content, eruption rate and instabilities of eruption regime in silicic volcanos. Earth Planet. Sci. Lett. 102, 413–429.
Kennedy, M.R., Pozrikidis, C., Skalak, R., 1994. Motion and deformation of liquid drops, and the rheology of dilute emulsions in simple shear flow. Comp. Fluids 23, 251–278.
Kilburn, C.R.J., Guest, J.E., 1993. Aa lavas of Mount Etna, Sicily. In: Kilburn, C. (Ed.), Active Lavas. pp. 73–106.
Klug, C., Cashman, K.V., 1996. Permeability development in vesiculating magmas—implications for fragmentation. Bull. Volcanol. 58, 87–100.
Laidley, R.A., McKay, D.S., 1971. Geochemical examination of obsidians from Newberry Caldera, Oregon. Contrib. Mineral. Petrol. 30, 336–342.
Lange, R.A., 1994. The effect of $H_2O$, $CO_2$, and F on the density and viscosity of silicate melts. In: Carroll, M.R., Holloway, J.R. (Eds.), Volatiles in Magmas. Mineral. Soc. Am. Rev. in Mineral. 30, pp. 331–369.
Leal, L.G., 1992. Laminar Flow and Convective Transport Processes. Butterworth-Heinemann.
Lipman, P.W., Banks, N.G., 1987. Aa flow dynamics, Mauna Loa 1984 (Hawaii). U.S. Geol. Surv. Prof. Pap. 1350, 1527–1567.
Loewenberg, M., Hinch, E.J., 1996. Numerical simulation of a concentrated emulsion in shear flow. J. Fluid Mech. 321, 395–419.
Loewenberg, M., Hinch, E.J., 1997. Collision of two deformable drops in shear flow. J. Fluid Mech. 338, 299–315.
MacDonald, G.A., 1954. Activity of Hawaiian volcanoes during the years 1940–50. Bull. Volcanol. 16, 119–179.
Manga, M., 1997. Interactions between mantle diapirs. Geophys. Res. Lett. 24, 1871–1874.
Manga, M., Stone, H.A., 1993. Buoyancy-driven interactions between deformable drops at low Reynolds numbers. J. Fluid Mech. 256, 647–683.
Manga, M., Stone, H.A., 1995. Collective hydrodynamics of deformable drops and bubbles in dilute suspensions at low Reynolds numbers. J. Fluid Mech. 300, 231–263.
McBirney, A.R., 1993. Igneous Petrology. Jones and Bartlett Publishers, Boston.
Murase, T., McBirney, A.R., 1973. Properties of some common igneous rocks and their melts at high temperatures. Geol. Soc. Am. Bull. 84, 3563–3592.
Nakada, S., Motomura, Y., Shimizu, H., 1995. Manner of ascent an Unzen volcano (Japan). Geophys. Res. Lett. 22, 567–570.
Neal, C.A., McGimsey, R.G., Gardner, C.A., Michelle, L.H., Nye, C.J., 1995. Tephra-fall deposits from the 1992 eruptions of Crater Peak, Mount Spurr Volcano, Alaska: a preliminary report on distribution, stratigraphy, and composition. U.S.G.S. Bull. B 2139, 65–79.
Pinkerton, H., Norton, G., 1995. Rheological properties of basaltic lavas at sub-liquidus temperatures: laboratory and field measurements on lavas from Mount Etna. J. Volcanol. Geotherm. Res. 68, 307–323.
Pinkerton, H., Stevenson, R.J., 1992. Methods of determining the rheological properties of magmas at sub-liquidus temperatures. J. Volcanol. Geotherm. Res. 53, 47–66.
Pinkerton, H., Herd, R.A., Kent, R.M., 1996, Field measurements of the rheological properties of basaltic lavas on Kilauea, Hawaii. Abstract from the Chapman Conf. on Long Lava Flows.
Polacci, M., Papale, P., 1997. The evolution of lava flows from ephemeral vents at Mount Etna: Insights from vesicle distribution and morphological studies. J. Volcanol. Geotherm. Res. 76, 1–17.
Pozrikidis, C., 1992, Boundary Integral and Singularity Methods for Linearized Viscous Flow. Cambridge Univ. Press.
Pozrikidis, C., 1993. On the transient motion of ordered suspensions of liquid drops. J. Fluid Mech. 246, 301–320.
Rallison, J.M., 1984. The deformation of small viscous drops and bubbles in shear flows. Annu. Rev. Fluid Mech. 16, 45–66.
Rallison, J.M., Acrivos, A., 1978. A numerical study of the

deformation and burst of a drop in an extensional flow. J. Fluid Mech. 89, 191–209.

Ramsay, J.G., Huber, M.I., 1987. The techniques of modern structural geology. Academic Press, London.

Roscoe, R., 1952. The viscosity of suspensions of rigid spheres. Br. J. Appl. Phys. 3, 267–269.

Russel, W.B., Saville, D.A., Schowalter, W.R., 1989. Colloidal Dispersions. Cambridge Univ. Press.

Rutherford, M.J., Hill, P.M., 1993. Magma ascent rates from amphibole breakdown—an experimental study applied to the 1980–1986 Mount St-Helens eruptions. J. Geophys. Res. 98, 19667–19685.

Schowalter, W.R., Chaffey, C.E., Brenner, H., 1968. Rheological behaviour of a dilute emulsion. J. Colloid Interface Sci. 26, 152–160.

Shaqfeh, E.S.G., Fredrickson, G.H., 1990. The hydrodynamic stress in a suspension of rods. Phys. Fluids 2, 7–24.

Shaw, H.R., 1972. Viscosities of magmatic silicate liquids: an empirical method of prediction. Am. J. Sci. 272, 870–893.

Shaw, H.R., Wright, T.L., Peck, D.L., Okamura, R., 1968. The viscosity of basaltic magma: an analysis of field measurements in Makaopuhi lava lake Hawaii. Am. J. Sci. 266, 225–264.

Sibree, J.O., 1933. The viscosity of froth. Trans. Faraday Soc. 28, 325–331.

Spera, F.J., Borgia, A., Strimple, J., Feigenson, M.D., 1988. Rheology of melts and magmatic suspensions: design and calibration of concentric cylinder viscometer with application to rhyolitic magma. J. Geophys. Res. 93, 10273–10294.

Stein, D.J., Spera, F.J., 1992. Rheology and microstructure of magmatic emulsions—theory and experiments. J. Volcanol. Geotherm. Res. 49, 157–174.

Stevenson, R.J., Briggs, R.M., Hodder, A.P.W., 1993. Emplacement history of a low-viscosity, fountain-fed pantelleritic lava flow. J. Volcanol. Geotherm. Res. 57, 39–56.

Stone, H.A., 1994. Dynamics of drop deformation and breakup in viscous fluids. Annu. Rev. Fluid Mech. 26, 65–102.

Taylor, G.I., 1932. The viscosity of a fluid containing small drops of another fluid. Proc. R. Soc. London A 138, 41–48.

Taylor, G.I., 1934. The formation of emulsions in definable fields of flow. Proc. R. Soc. Lond. A 146, 501–523.

Webb, S.L., Dingwell, D.B., 1990. Non-Newtonian rheology of igneous melts at high stresses and strain rates: Experimental results for rhyolite, andesite, basalt, and nephelinite. J. Geophys. Res. 95, 15695–15701.